Three-dimensional critical behavior and anisotropic magnetic entropy change in quasi-two-dimensional $LaCrSb_3$

Xiaojun Yang [*], Junxiao Pan, Weizhuo Gai, Yaping Tao, Hong Jia, Leiming Cao, and Yan Cao
College of Physics and Electronic Information, Luoyang Normal University, Luoyang 471022, China

(Received 29 September 2021; revised 10 December 2021; accepted 19 January 2022; published 26 January 2022)

The critical properties and magnetic entropy change of quasi-two-dimensional $LaCrSb_3$ single crystals have been systematically investigated. The ferromagnetic transition is determined to be of a second order. Critical exponents $\beta = 0.298(7)$ with a critical temperature $T_c = 132.0(2)$ K and $\gamma = 1.277(9)$ with $T_c = 132.5(3)$ K are yielded by the modified Arrott plot, whereas $\delta = 5.28(9)$ is deduced by a critical isotherm analysis at $T = 132$ K. The critical exponents of quasi-two-dimensional $LaCrSb_3$ exhibit a three-dimensional critical behavior. The magnetic interaction is found to be of a long range and the magnetic exchange distance decays as $J(r) \approx r^{-4.9}$, which lies between the mean-field model and 3D Heisenberg model. Furthermore, the magnetic entropy change $-\Delta S_M$ features a maximum around T_c, i.e., $-\Delta S_M^{\max} \sim 3.4$, 5.9, and 5.8 J kg^{-1} K^{-1} for a field change of 5 T applied the $H//a$, b, and c axes, respectively. The rotating magnetic entropy change $\Delta S_M^R(T, H)$ between the a and b axes (the a and c axes) reaches a maximum value of 2.55 (2.49) J kg^{-1} K^{-1} around T_c, exhibiting strong anisotropic features. However, $\Delta S_M^R(T, H)$ between the b and c axes is ∼0 J kg^{-1} K^{-1} at $T > T_c$ displaying a nearly isotropic behavior, and is less than 0.3 J kg^{-1} K^{-1} at $T < T_c$ showing weak anisotropy.

DOI: 10.1103/PhysRevB.105.024419

I. INTRODUCTION

Attracting researchers' long-standing interest, layered transition-metal materials have been extensively investigated due to the exotic physical properties, such as the high-temperature superconductivity in copper- and iron-based superconductors [1–3], the high thermoelectric powder in cobaltites [4,5], and the large magnetoresistance (MR) in manganites [6]. Remarkably, the recent discovery of intrinsic long-range magnetic order in two-dimensional (2D) ferromagnets, such as $CrGeTe_3$, CrI_3, Fe_3GeTe_2, $MnSe_2$, $FePS_3$, and VSe_2 [7–14], have not only provided potential platforms for designing novel spin-related devices but also refreshed the famous fundamental theory that the ferromagnetic (FM) order in 2D systems would be destroyed by thermal fluctuation and collapse at a finite temperature [15].

Crystallized in an orthorhombic structure with a *Pbcm* space group (no. 57), $LaCrSb_3$ possesses a quasi-2D crystal structure consisting of infinite LaSb and $CrSb_2$ layers stacked along the a axis (inset of Fig. 1) [16–19]. A surprising property of this system is the presence of a coexistence of localized and itinerant spins in a pure d-electron compound with an antiferromagnetic (AFM) Néel temperature ($T_N = 98$ K) less than the FM Curie temperature ($T_C = 132$ K), and the AFM transition is suppressed with a rather small magnetic field $\mu_0 H \sim 0.025$ T, leading to a surprisingly rich phase diagram [16,20]. Furthermore, the recent investigations on the anomalous Hall conductivity (AHC) of $LnCrSb_3$ (Ln = La, Ce, and Nd) suggest the existence of a strong Berry curvature, which is induced by abundant momentum-space crossings and narrow energy-gap openings, providing an intriguing system for investigations on nontrivial band topologies [21]. To achieve the modulation of the promising topological properties by magnetization, the clarification of the magnetic interactions of $LaCrSb_3$ is of essential importance. In particular, the critical behavior of $LaCrSb_3$, which could provide insight into the nature of spin dimensionality, correlation length, magnetic interactions, and the spatial decay of correlation function at criticality [22–25], is still absent and deserves a detailed investigation.

In the present work, we studied the critical behavior as well as the magnetic entropy change of $LaCrSb_3$ single crystal. Self-consistent critical exponents are acquired by various methods. A 3D critical behavior is unveiled. The reliability of the critical exponents are checked by scaling analyses. The magnetic interaction is of a long range and the magnetic-exchange distance is found to decay as $J(r) = r^{-4.9}$, which lies between the 3D Heisenberg model and the mean-field model. The magnetic entropy changes exhibit strong magnetic anisotropy along the a axis and a nearly isotropic behavior in the bc plane. The rescaled $-\Delta S_M(T, H)$ curves can well fall into a universal curve, confirming its nature of a second order. The systematical investigation on the critical exponents, the magnetic interaction, and the anisotropy of the interesting compound $LaCrSb_3$ could help us in further fully understanding the discovered nontrivial properties, such as AHC.

II. EXPERIMENTAL DETAILS

Single crystals of $LaCrSb_3$ were prepared by a self-flux method. The ingots of the La (99.9%), powders of Cr (99.9%), and powders of Sb (99.9%) were mixed in an atomic ratio of 1 : 2 : 20. The mixtures were placed in a high quality

[*]xiaojunyang01@foxmail.com

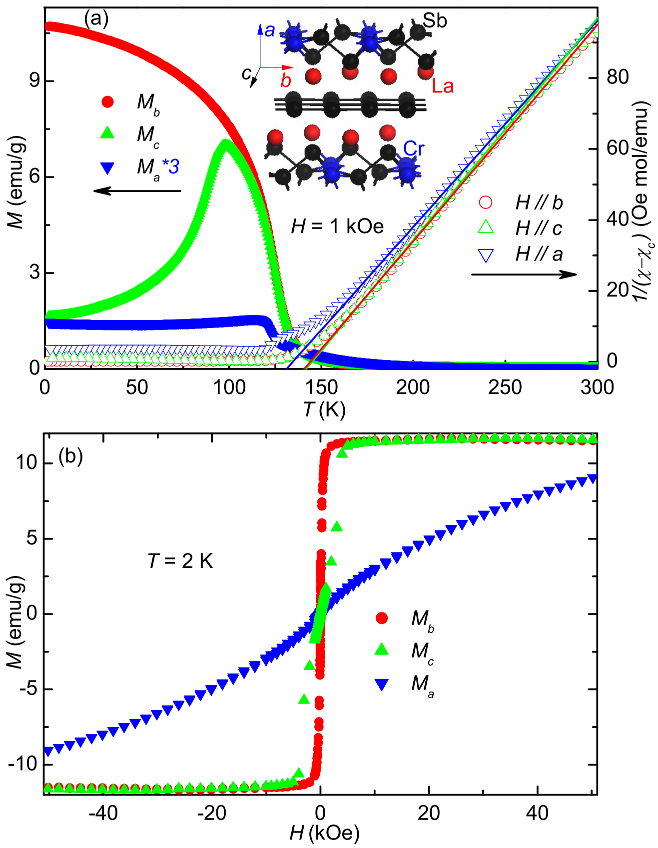

FIG. 1. (a) Left: Temperature dependence of magnetization curves under $H = 1$ kOe applied along three different axes. Right: plots of $1/(\chi - \chi_c)$ vs T under a 1 kOe field applied along three different axes. The linear lines display the fitting by the Curie-Weiss law. Inset: Crystal structure of $LaCrSb_3$. (b) $M(H)$ curves along three different axes at $T = 2$ K.

alumina crucible and subsequently sealed in a quartz tube. The tube was heated to 1373 K over 10 h and then cooled at a rate of 3 K/h to 923 K, at which point the Sb flux was spun off using a centrifuge. The resulting crystals were rectangular planes with a thin face parallel to the a axis and the longest side parallel to the c axis, and the typical sizes are $a : b : c = 0.2 : 0.9 : 1.5$ mm. The magnetic properties were taken with a commercial superconducting quantum interference device (SQUID) magnetometer (MPMS, Quantum Design).

III. RESULTS AND DISCUSSION

A. Magnetic properties

The field-cooled magnetization as a function of temperature $M(T)$ under $H = 1$ kOe along the a, b, and c axis is presented in the left axis of Fig. 1(a). Obviously, the magnetization $M(T)$ along different crystalline directions exhibits an anisotropic behavior, consistent with the low dimensional character of $LaCrSb_3$. A FM transition is detected at $T_c \sim 132$ K, and the b (a) axis is the easy (hard) magnetization direction. As the field applied along c axis $H\|c$, a decrease in magnetization is found below $T^* = 98$ K, implying a possible AFM ground state and complex anisotropic magnetic structure, which should be associated with a spin reorientation [16]. The temperature dependence of magnetic susceptibility $\chi = M/H$ for $T > 170$ K can be well characterized by the Curie-Weiss law [Fig. 1(a)], $\chi = \chi_c + C/(T - \theta)$, where χ_c is a temperature-independent term, θ is the Weiss temperature, and C denotes the Curie-Weiss constant. The Weiss temperatures yielded by the Curie-Weiss fitting are $\theta_a = 134.8$ K, $\theta_b = 144.3$ K, and $\theta_c = 145.2$ K for $H\|a$, $H\|b$, and $H\|c$, respectively, with the positive values demonstrating the ferromagnetic interaction between Cr ions. The effective moments $\mu_{\text{eff}} = 3.71$, 3.62, and $3.57\mu_B$/f.u., acquired by fitting the $H\|a$, $H\|b$, and $H\|c$ data, respectively. The values of μ_{eff} are comparable with the theoretically expected values for Cr^{3+} of $3.87\mu_B$. The field-dependent magnetization $M(H)$ at $T = 2$ K is shown in Fig. 1(b). At $H = 50$ kOe the saturated magnetization of $H\|a$, $H\|b$, and $H\|c$ are $\mu_s = 0.90$, 1.17, and $1.17\mu_B$/f.u., respectively. When the field is along the easy-magnetization axis (b axis), the saturation appears immediately almost as a steplike function to $\mu_b = 1.17\mu_B$/f.u. A bump in the magnetization of $H\|c$ axis is found under $H \sim 3$ kOe, which should be related to the downturn of M_c observed in Fig. 1(a). The c axis magnetization μ_c then saturates to approximately the same value as μ_b, implying the possible antiferromagnetic ground state is suppressed and driven to FM with a field of about $H = 4$ kOe. The magnetization along the a axis exhibits differently from the previous two, and continues to increase almost linearly up to the maximum measured field of 50 kOe. Within the bc plane, the magnetization is found to be isotropic at $H > 4$ kOe, but along the a axis the magnetization is unique.

TABLE I. Weiss temperatures, effective moments, saturated moments, and the Rhodes-Wohlfarth ratio of $LaCrSb_3$.

Axis	θ (K)	μ_{eff} (μ_B)	μ_s (μ_B)	RWR
$H\|a$	134.8	3.71	0.9	3.2
$H\|b$	144.3	3.62	1.17	2.4
$H\|c$	145.2	3.57	1.17	2.3

The obtained magnetic parameters of $LaCrSb_3$ are sumarized in Table I. Then we can evaluate the Rhodes-Wohlfarth ratio (RWR), which is equal to P_c/P_s, where P_c is related to the effective moment, $P_c(P_c + 2) = \mu_{\text{eff}}^2$, and P_s denotes the saturated moment (μ_s) measured in the high field and low temperature ordered state [26,27]. RWR equals 1 in a localized system and becomes larger in an itinerant system. Here we calculated that RWR equals 3.2, 2.4, and 2.3 with $H\|a$, $H\|b$, and $H\|c$, respectively, suggesting an itinerant characterization and/or strong spin fluctuations in the ground state, which is consistent with previous reports [16,28]. Based on the Stoner criterion [29], $UD(\varepsilon_F) > 1$, where U and $D(\varepsilon_F)$ are Coulomb repulsion and the density of state (DOS) at the Fermi level, respectively, itinerant ferromagnetism can be affected by tuning U and/or $D(\varepsilon_F)$. Diverse ferromagnetic transition temperatures in $LaCrSb_3$ were observed at $T_c = 125$ K [19], $T_c = 142$ K [30], and $T_c = 132$ K [16], with the difference possibly due to diverse subtle disorders arising from the sample growth procedures [16].

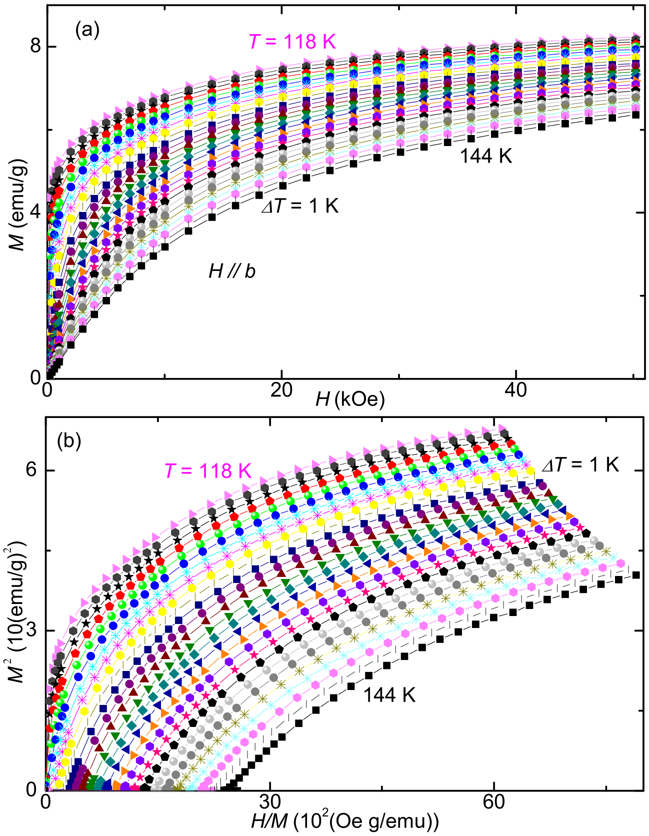

FIG. 2. (a) The field dependence of isothermals $M(H)$ measured under $H\|b$ from $T = 118$ to 144 K. (b) The Arrott plots of M^2 vs H/M for $H\|b$.

B. Critical behavior

The critical behavior of a system with a second-order phase transition provides insight into the origin of the the spin dimensionality, magnetic interactions, the correlation length, and the spatial decay of the correlation function at criticality [22–25]. According to the phase transition theory by Landau, the Gibbs free energy G of a paramagnetic (PM)–FM transition can be calculated as the following equation:

$$G(T, M) = G_0 + \frac{a}{2}M^2 + \frac{b}{4}M^4 - MH, \tag{1}$$

where a and b are temperature-dependent coefficients, and the equilibrium magnetization M denotes the order parameter. With equilibrium $\partial G/\partial M = 0$ (i.e., energy minimization), the magnetic equation of state is expressed as

$$H/M = a + bM^2. \tag{2}$$

Thus, the plots of M^2 vs H/M (the Arrott plot) should appear as parallel straight lines for different temperatures above and below T_c in the high field region [31]. To provide further insight into the nature of the FM transition in $LaCrSb_3$, the isothermal magnetization $M(H)$ along $H\|b$ around T_c is measured and representative $M(H)$ curves from $T = 118$ to 144 K with a temperature interval of 1 K are presented in Fig. 2(a). The curves of the Arrott plot are not parallel at the high-field region [Fig. 2(b)], recommending that the mean-field theory is not suitable for $LaCrSb_3$. According to the Banerjee criterion [32], the positive slopes of M^2 vs H/M curves in the vicinity of the PM-FM transition suggest a second-order phase transition in $LaCrSb_3$.

To acquire the critical parameters, we exploit the modified Arrott plot. For a second-order transition, its critical behavior can be described in detail by a series of interrelated critical exponents. In the vicinity of a second-order phase transition, the divergence of the correlation length $\xi = \xi_0|(T - T_c)/T_c|^{-\nu}$ results in universal scaling laws for the spontaneous magnetization M_s and the inverse initial magnetic susceptibility χ_0^{-1}. The mathematical definitions of the exponents can be expressed as [33,34]

$$M_s(T) \propto |\varepsilon|^{\beta}, \quad \varepsilon < 0, \quad T < T_c, \tag{3}$$

$$M \propto H^{1/\delta}, \quad \varepsilon = 0, \quad T = T_c, \tag{4}$$

$$\chi_0^{-1}(T) \propto |\varepsilon|^{\gamma}, \quad \varepsilon > 0, \quad T > T_c, \tag{5}$$

where $\varepsilon = (T - T_c)/T_c$ is the reduced temperature and parameters β (associated with M_s), δ (associated with magnetization at T_c), and γ (associated with χ_0^{-1}) are critical exponents. Several universal classes of models are exploited to establish the modified Arrott plots, and the 2D Ising model ($\beta = 0.125$, $\gamma = 1.75$), the 3D Ising model ($\beta = 0.325$, $\gamma = 1.24$), 3D Heisenberg model ($\beta = 0.365$, $\gamma = 1.386$), and tricritical mean-field model ($\beta = 0.25$, $\gamma = 1.0$) are displayed in Figs. 3(a)–3(d). In order to discover which model is the best, normalized slopes (NSs), defined as $S_N = S(T)/S(T_c)$ [where $S(T)$ denotes the slope of $M^{1/\beta}$ vs $(H/M)^{1/\gamma}$], are presented in Fig. 4. Because the modified Arrott plot should consist of various parallel straight lines, all values of NS should be equal to 1.0 in an ideal model. Apparently, the critical behavior of $LaCrSb_3$ does not belong to any universal classes. A self-consistent iterative method was exploited to generate the modified Arrott plot [35–37]. The inset of Fig. 4 displays the high field region of the acquired modified Arrott plot of $M^{1/\beta}$ vs $(H/M)^{1/\gamma}$ around T_c for $LaCrSb_3$. This gives $M_s(T)$ and $\chi_0^{-1}(T)$ as the intercepts on the $M^{1/\beta}$ axis and $(H/M)^{1/\gamma}$ axis, respectively.

Figure 5(a) presents the temperature dependence of the final M_s and χ_0^{-1}. The critical exponents $\beta = 0.298(7)$ with $T_c = 132.0(2)$ K, and $\gamma = 1.277(9)$ with $T_c = 132.5(3)$ K are acquired by fitting Eqs. (3) and (5). Additionally, in the Kouvel-Fisher (KF) relation [38], i.e., $M_s(T)/[dM_s(T)/dT] = (T - T_c)/\beta$ and $\chi_0^{-1}(T)/[d\chi_0^{-1}(T)/dT] = (T - T_c)/\gamma$, linear fittings to the plots of $M_s(T)/[dM_s(T)/dT]$ and $\chi_0^{-1}(T)/[d\chi_0^{-1}(T)/dT]$ vs T in Fig. 5(b) generate $\beta = 0.294(8)$ with $T_c = 132.0(5)$ K, and $\gamma = 1.276(9)$ with $T_c = 132.4(5)$ K. The third exponent δ can be calculated from the Widom scaling relation [39],

$$\delta = 1 + \gamma/\beta. \tag{6}$$

Using β and γ yielded by the modified Arrott plot and the Kouvel-Fisher plot, $\delta = 5.29(13)$ and 5.34(15) are calculated, respectively, which are close to the direct fits of Eq. (4) at 132 K [$\delta = 5.28(9)$] [inset of Fig. 5(a)], demonstrating self-consistence and reliability of the achieved exponents.

Furthermore, the critical analyses for the $H\|c$ have been also performed. No visible differences between $H\|b$ and $H\|c$

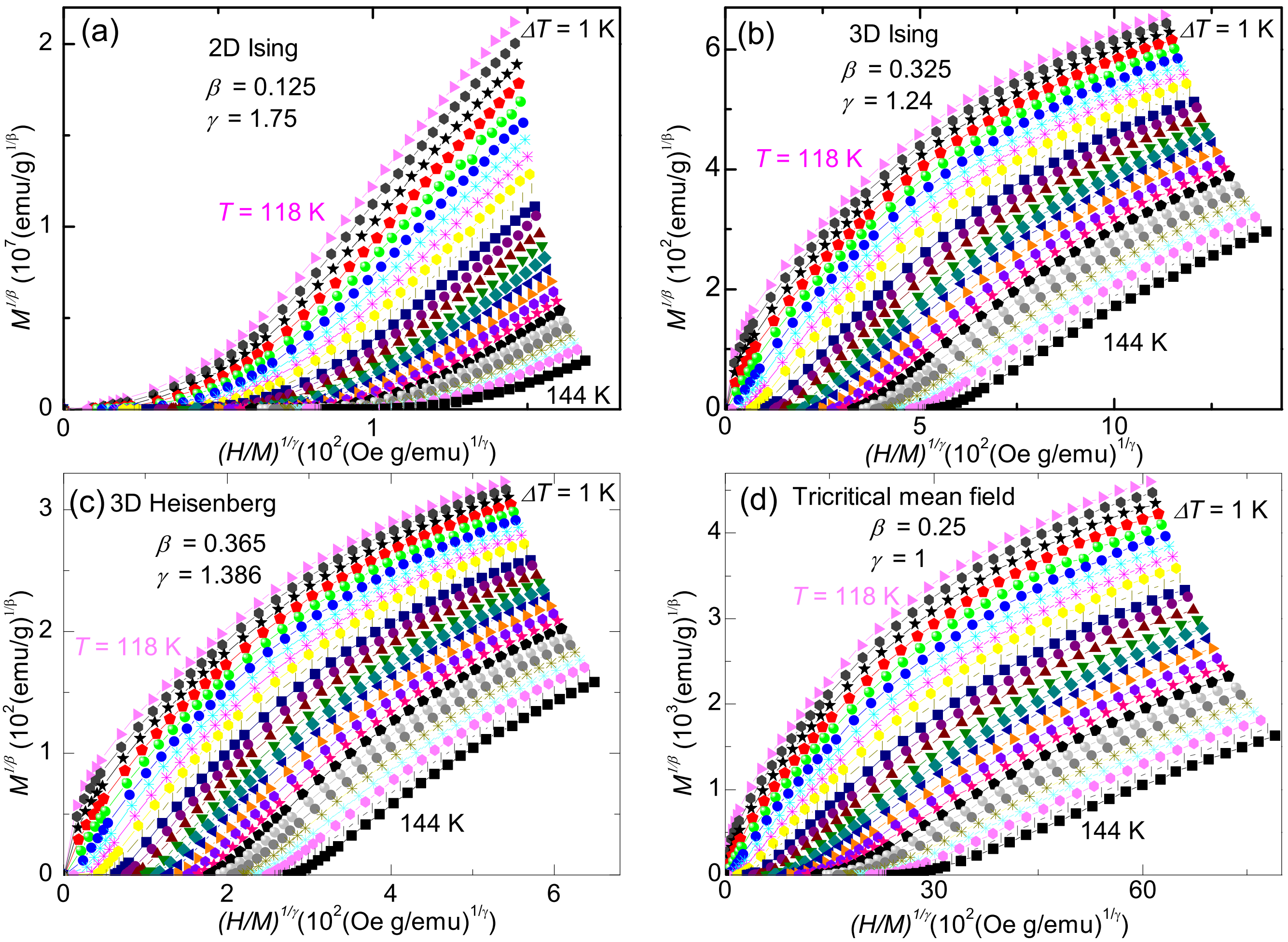

FIG. 3. The isotherms plotted as $M^{1/\beta}$ vs $(H/M)^{1/\gamma}$ with a (a) 2D Ising model, (b) 3D Ising model, (c) 3D Heisenberg model, and (d) tricritical mean-field model.

are detected in the Arrott plot and the modified Arrott plot within the error range of the experiment, implying an almost isotropic critical behavior between the b and c axes, which is consistent with the following analyses on the magnetic entropy change. The critical analyses consider the points around T_c, and the AFM-like transition presents below $T^* = 98$ K at $H \| c$, which will not make difference on the critical behavior around T_c.

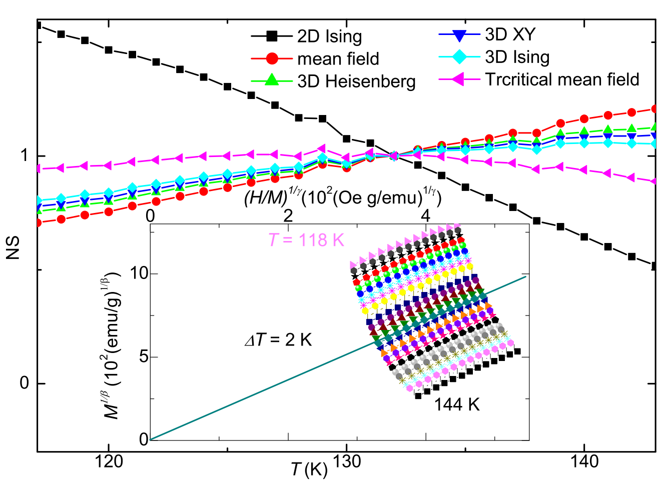

FIG. 4. Plots of normalized slopes $S_N = S(T)/S(T_c)$ vs T for diverse universal theoretical models. Inset: The modified Arrott plot of $M^{1/\beta}$ vs $(H/M)^{1/\gamma}$.

The scaling analysis can be exploited to check the reliability of the deduced critical exponents and T_c. In the critical asymptotic region, the magnetic equation can be written as [39]

$$M(H, \varepsilon) = \varepsilon^{\beta} f_{\pm}(H/\varepsilon^{\beta+\gamma}), \tag{7}$$

where f_+ for $T > T_c$ and f_- for $T < T_c$, respectively, represents regular functions. In terms of rescaled magnetization $m = M|\varepsilon|^{-\beta}$ and rescaled field $h = H|\varepsilon|^{-(\beta+\gamma)}$, the above equation can be reexpressed as $m = f_{\pm}(h)$, which implies that for appropriate scaling relations and properly chosen values of β, γ, and δ, scaled m vs h will fall into two universal branches: one above T_c and another below T_c. This is an important criterion for the critical exponents. Plots of m vs h are presented in Fig. 5(c) with a $\log_{10}$-$\log_{10}$ scale, and all the data collapse onto two separate branches. The scaling equation of state can also take another form [33],

$$\frac{M}{H^{\delta}} = g(X)\left(\frac{\varepsilon}{H^{1/\beta}}\right), \tag{8}$$

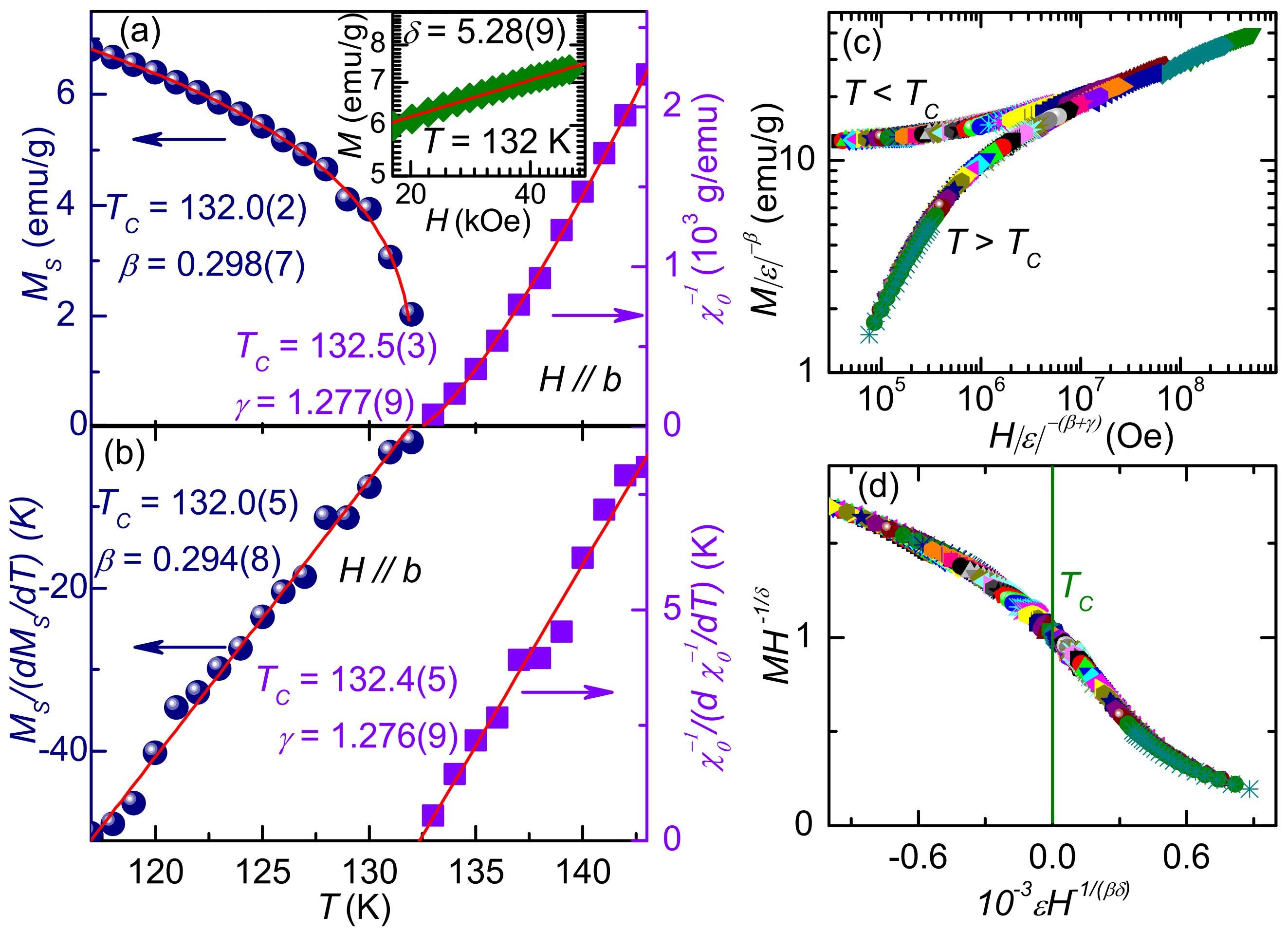

FIG. 5. (a) The spontaneous magnetization M_s (left) and the inverse initial susceptibility $1/\chi_0$ (right) as a function of the temperature with solid fitting curves for $LaCrSb_3$. Inset: Plots of M vs H at $T_c = 132$ K in $\log_{10}$-$\log_{10}$ scale with a linear fitting. (b) The Kouvel-Fisher plot of temperature-dependent $M_s(dM_s/dT)^{-1}$ (left) and $\chi_0^{-1}(d\chi_0^{-1}/dT)^{-1}$ (right). The T_c and critical exponents are deduced by linear fits (red lines). (c) Scaling plots of $M|\varepsilon|^{-\beta}$ vs $H|\varepsilon|^{-(\beta+\gamma)}$ in $\log_{10}$-$\log_{10}$ scale. (d) Renormalized plots of $M(H)$ curves by $MH^{-1/\delta}$ vs $\varepsilon H^{-1/(\beta\delta)}$.

where $g(x)$ is a scaling function. From Eq. (8), all the data should collapse onto a single curve. This is indeed observed, i.e., the plots of $MH^{-1/\delta}$ vs $\varepsilon H^{-1/(\beta\delta)}$ fall into a single curve with the T_c at the zero point of the horizontal axis. The well-renormalized curves further demonstrate the reliability of the generated critical exponents.

The critical exponents derived by various methods are summarized in Table II along with the theoretically predicted values for diverse models. The value of β for 2D magnets should be located in a universal window $0.1 \leqslant \beta \leqslant 0.25$ [41]. Apparently, the critical exponents of $LaCrSb_3$ exhibit a 3D critical behavior. The experimentally yielded critical

TABLE II. Comparison of critical exponents of $LaCrSb_3$ with various theoretical models. The MAP, KFP, CI, and MCE denote the modified Arrott plot, the Kouvel-Fisher plot, the critical isotherm, and the magnetocaloric effect, respectively.

Composition	Reference	Technique	β	γ	δ	n	m
$LaCrSb_3$	this work	MAP	0.298(7)	1.277(9)	5.29(13)		
	this work	KFP	0.294(8)	1.276(9)	5.34(15)		
	this work	CI			5.28(9)		
	this work	MCE	0.246(3)	2.04(3)	9.26(2)	0.670(5)	1.108(2)
Mean field	[31]	theory	0.5	1.0	3.0	0.667	1.333
2D Ising	[40]	theory	0.125	1.75	15	0.533	1.06
3D Ising	[31]	theory	0.325	1.24	4.82	0.569	1.207
3D Heisenberg	[31]	theory	0.365	1.386	4.8	0.637	1.208
Tricritical mean field	[32]	theory	0.25	1.0	5	0.4	1.20
3D *XY*	[31]	theory	0.345	1.316	4.81	0.606	1.208

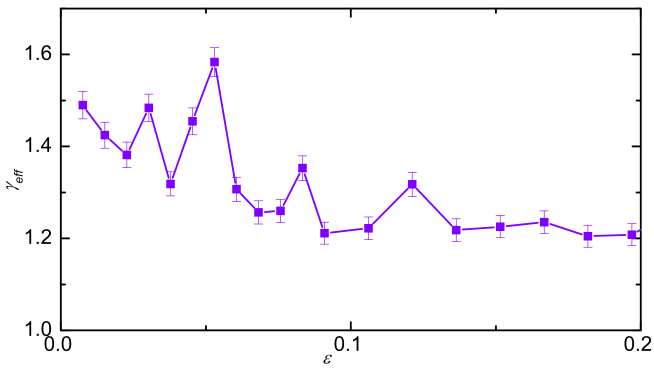

FIG. 6. Effective exponent γ_{eff} vs $\varepsilon = (T - T_c)/T_c$ above T_c.

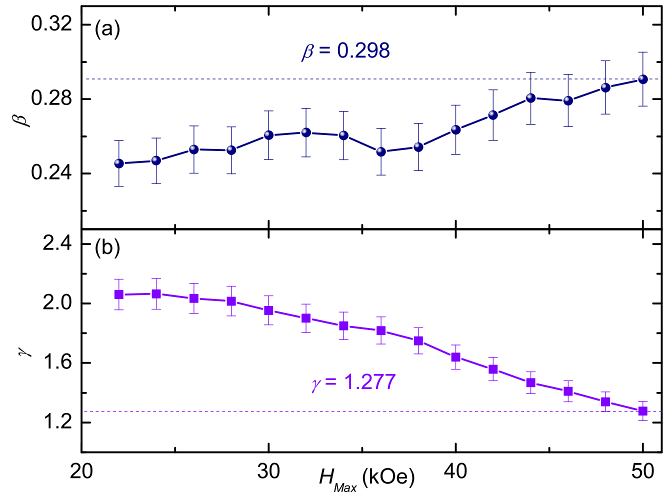

FIG. 7. Dependence of (a) β and (b) γ on the fitted maximum magnetic field.

exponents β, γ, and δ are close to, but show some deviation from, the theoretical values of the 3D Ising model. The 3D features of $LaCrSb_3$ could be associated with the magnetocrystalline anisotropy. According to the theory by Mermin-Wagner, magnetic order should not appear in ideal low dimensional systems at finite temperature due to thermal fluctuation [15,42]. When anisotropic magnetism takes place, however, this conclusion does not necessarily take effect. In the case of $LaCrSb_3$, despite the crystal structure exhibits two-dimensional features, the existence of magnetocrystalline anisotropy could induce the stabilization of the ferromagnetism. Nonzero values of the inverse magnetic susceptibility are observed above the T_c [Fig. 1(a)], demonstrating ferromagnetic correlations in the paramagnetic region, which implies the ferromagnetic correlations could take effect even above T_c [43–45]. To provide further insight into the critical exponents above T_c, we calculated the effective exponent, $\gamma_{\mathrm{eff}} = d[\ln\chi_0^{-1}(\varepsilon)]/d(\ln\varepsilon)$. As presented in Fig. 6, γ_{eff} exhibits a tendency of decreasing almost monotonically with an increasing ε, indicating a crystalline FM [46,47]. For comparison, γ_{eff} usually exhibits a nonmonotonic temperature dependence in disordered systems, implying the effect from the random distribution of magnetic elements and/or the clusters should not be dominant in $LaCrSb_3$ [48–50].

It is worthwhile to note that both the range of temperature around the T_c and the magnetic field range chosen could take effect on the generated exponents. While much is known on the temperature dependence of critical exponents, the influence of magnetic field on critical exponents in ferromagnets is not often discussed [50,51]. The modified Arrott plot processes described above are repeated for H_{Max} - 20 kOe $< H \leqslant H_{\mathrm{Max}}$, and the generated critical exponents are illustrated in Figs. 7(a) and 7(b). As the fitted range decreases to lower fields, the β drops to the values close to 0.25, which is on the border of 2D to 3D critical behavior, probably due to the 2D crystalline structure and the magnetocrystalline anisotropy. Moreover, the decrease in γ is large and systematic as the maximum magnetic field is increased.

Then, we discuss the nature as well as the range of interactions in $LaCrSb_3$. On the basis of the renormalization-group theory, the interaction decays with distance r as $J(r) \sim r^{-(3+\sigma)}$, where σ is associated with the range of the interaction [52], which is short or long depending on $\sigma > 2$ or $\sigma < 2$. The exponent γ is calculated as [35,52,53],

$$\gamma = 1 + \frac{4}{d}\frac{(n+2)}{(n+8)}\Delta\sigma + \frac{8(n+2)(n-4)}{d^2(n+8)^2} \times \left(1 + \frac{2G(\frac{d}{2})(7n+20)}{(n-4)(n+8)}\right)\Delta\sigma^2, \tag{9}$$

where $\Delta\sigma = \sigma - d/2$, $G(\frac{d}{2}) = 3 - \frac{1}{4}(\frac{d}{2})^2$, and n denotes the spin dimensionality. When $\sigma = 2$, the Heisenberg model is effective for a 3D isotropic magnet, where $J(r)$ decays faster than r^{-5}. When $\sigma = 3/2$, the mean-field model is valid and $J(r)$ decays slower than $r^{-4.5}$. In the case of $LaCrSb_3$, it is discovered that the magnetic exchange decays with distance as $J(r) = r^{-4.9}$, which lies between that of the mean-field mode and the 3D Heisenberg model with a long-range interaction [35,52,53].

In addition, the critical behavior of 2D and quasi-2D Cr-based magnetic materials has been extensively investigated. For instance, the magnetism of CrI_3 follows the crossover behavior of a 3D-Ising behavior with mean field type interactions [54], $CrSiTe_3$ displays a 2D-Ising ferromagnetic behavior [55], $CrGeTe_3$ exhibits a tricritical mean-field model [56], and $Cr_{1/3}NbS_2$ shows a 3D Heisenberg-like ferromagnetism [57]. The diverse critical behavior could come from the inevitable different interlayer coupling and the magnetic anisotropy [54]. Moreover, the localized or itinerant nature of the Cr moments should also take effect on the range of the ferromagnetic interaction [57].

C. Magnetic entropy change

The magnetic entropy change $\Delta S_M(T, H)$ induced by the external field is expressed as the following equation:

$$\Delta S_M(T, H) = \int_0^H \left(\frac{\partial M}{\partial T}\right)_H dH. \tag{10}$$

Figures 8(a)–8(c) present the calculated magnetic entropy change as a function of temperature [$-\Delta S_M(T)$] under various fields with $H\|a$, $H\|b$, and $H\|c$, respectively. A peak around T_c occurs at each curve, and the maximum value of

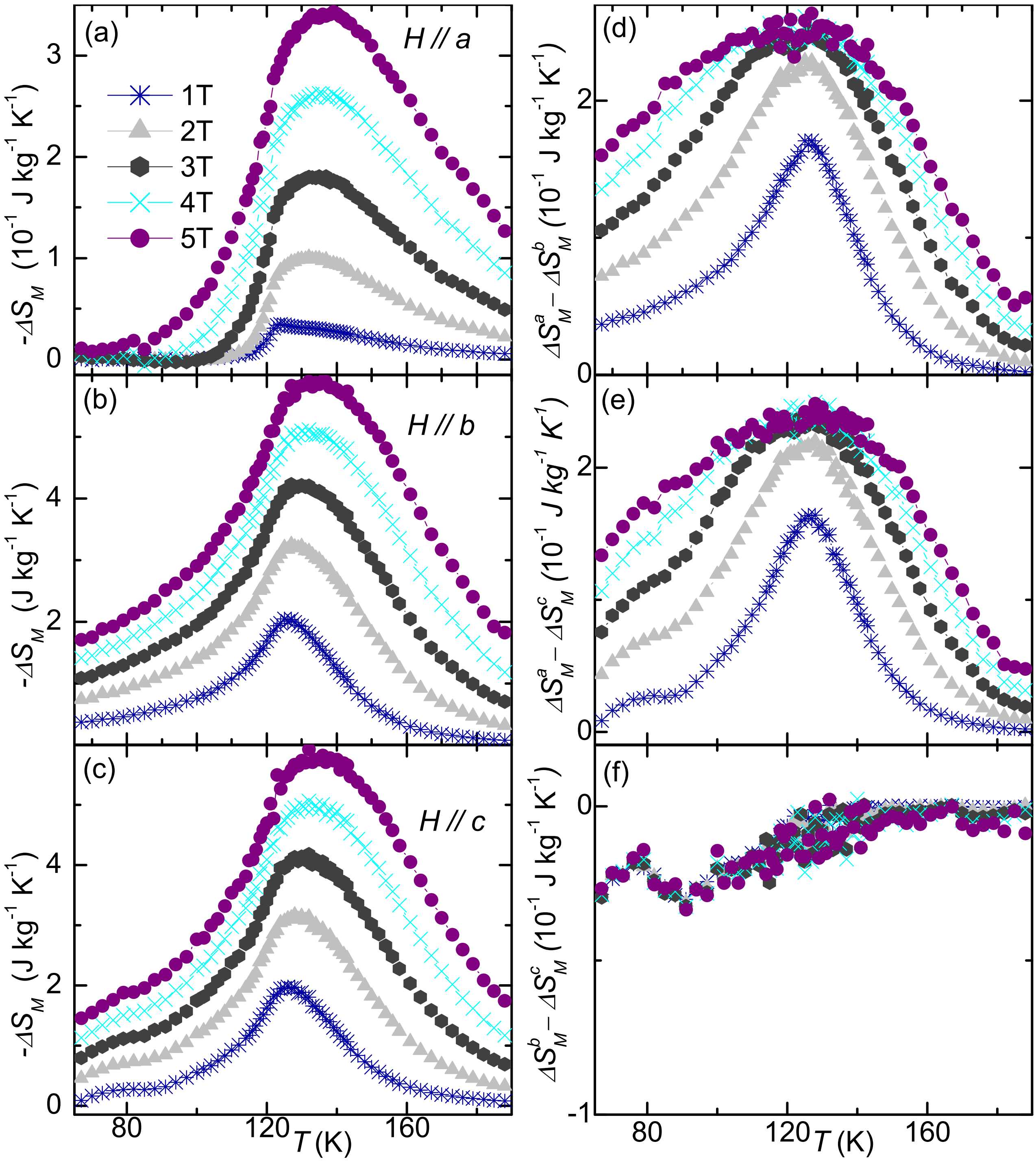

FIG. 8. (a)–(c) Calculated magnetic entropy change of $LaCrSb_3$ for the magnetic field along three different axes, respectively. (d)–(f) Calculated rotating magnetic entropy change of $LaCrSb_3$ between the (d) a and b axes, (e) a and c axes, and (f) b and c axes, respectively.

the $-\Delta S_M$ reaches 3.4, 5.9, and 5.8 J kg^{-1} K^{-1} for the $H\|a$, b, and c axes, respectively; and there exist small shifts of the $-\Delta S_M^{\max}$ peaks towards higher temperatures with an increasing of the magnetic field, which excludes the mean-field model [37,58,59], consistent with the above critical-behavior analysis. For the $H\|a$ axis, the temperature dependence of $-\Delta S_M$ exhibits negative values below 4 T at temperature below T_c, which should originate from the competition between the temperature dependence of magnetic anisotropy and the magnetization [60,61]. To provide further insight into the anisotropy of the magnetization, we calculated the rotating magnetic entropy change $-\Delta S_M^R$, which is expressed as [62]

$$\Delta S_M^R(T, H) = \Delta S_M(T, H_a) - \Delta S_M(T, H_b). \qquad (11)$$

As displayed in Figs. 8(d) and 8(e), $\Delta S_M^R(T, H)$ between the a and b axes (a and c axes) reach maximum values of 2.55 (2.49) J kg^{-1} K^{-1} around T_c, respectively, exhibiting strong anisotropic features. However, $\Delta S_M^R(T, H)$ between the

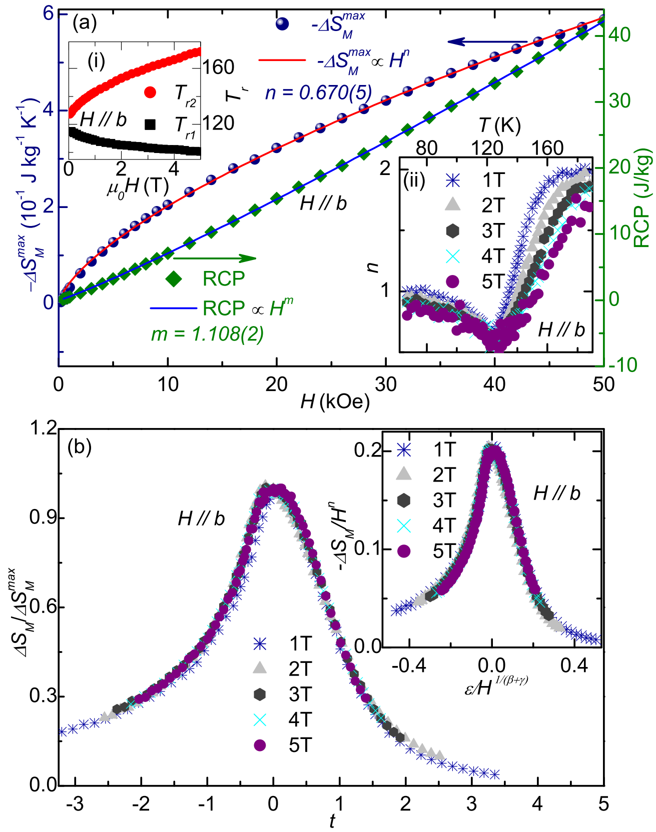

FIG. 9. (a) The field dependence of $\Delta S_M^{\max}$ and RCP for $H \| b$. Inset (i): Field-dependent T_{r1} and T_{r2}; (ii) the temperature dependence of n under various fields. (b) The normalized magnetic entropy change $\Delta S_M/\Delta S_M^{\max}$ as a function of the reduced temperature t. Inset: Scaling of $\Delta S_M(T)$ under the obtained critical exponents.

b and c axes is ∼0 J kg^{-1} K^{-1} at $T > T_c$ displaying a nearly isotropic behavior, and is less than 0.3 J kg^{-1} K^{-1} at $T < T_c$ showing weak anisotropy [Fig. 8(f)]. Under $H \| c$, small cusps at ∼90 K can be observed in Figs. 8(c) and 8(e), which should be related to the spin reorientation transition.

The parameters of $-\Delta S_M$ curves follow a series of power-law dependencies on the field as the following equations [63]:

$$-\Delta S_M^{\max} \propto H^n, \tag{12}$$

$$\text{RCP} \propto H^m, \tag{13}$$

where $-\Delta S_M^{\max}$ denotes the maximum value of the $-\Delta S_M$, RCP is the relative cooling power, which is calculated as $-\Delta S_M^{\max} \times \delta_{\text{FWHM}}$ (δ_{FWHM} is the full width at half maximum of $-\Delta S_M$), and n and m are related to the critical exponents as follows [64,65]:

$$n(T_c) = 1 + (\beta - 1)/(\beta + \gamma), \tag{14}$$

$$m = 1 + 1/\delta. \tag{15}$$

The left and right axes of Fig. 9(a) plot the field dependence of $-\Delta S_M^{\max}$ and RCP with $H \| b$, where the fitted curves by Eqs. (12) and (13) yield $n = 0.670(5)$ and $m = 1.108(2)$, respectively. The inset (ii) of Fig. 9(a) presents the plots of $n(T)$ in various fields, which exhibits typical behavior of a ferromagnetic system [66], i.e., at low temperatures, well below T_c, n approaches 1; at high temperature, well above T_c, n reaches 2 as a consequence of the Curie-Weiss law; at $T = T_c$, n has a minimum.

According to Eqs. (6), (15), and (14), the critical exponents can be calculated as $\beta = 0.246(3)$, $\gamma = 2.04(3)$, and $\delta = 9.26(2)$. The above method based on the magnetic entropy change directly generates the critical exponents, which stays away from the deviation caused by the multistep nonlinear fitting in the modified Arrot plot and KF method [61,67]. For comparison, the generated critical exponents of $LaCrSb_3$ with various methods are summarized in Table II. As we can see, there exists a discrepancy of critical exponents via various methodologies. The discrepancy is commonly found in $CrSbSe_3$ [62], $Fe_{3-x}GeTe_2$ [67], and VI_3 [61], which could come from the different fitting regions [61,68].

The temperature-dependent magnetic entropy change $-\Delta S_M(T, H)$ of a second-order magnetic transition can be normalized to a universal curve independent of the external field. The magnetic entropy change is scaled as $\Delta S'_M = \Delta S_M/\Delta S_M^{\max}$, and the temperature is scaled into a renormalized temperature t defined as [69]

$$t_- = (T_c - T)/(T_{r1} - T_c), \quad T \leqslant T_c, \tag{16}$$

$$t_+ = (T - T_c)/(T_{r2} - T_c), \quad T > T_c, \tag{17}$$

where T_{r1} and T_{r1}, which are presented in inset (i) of Fig. 9(a), denote two reference temperatures of the full width at half maximum, i.e., $\Delta S_M(T_{r1}, T_{r2}) = \frac{1}{2}\Delta S_M^{\max}$. The scaled $\Delta S'_M$ vs scaled t curves under $H \| b$ are displayed in Fig. 9(b). All plots under diverse H fall into a single universal curve. For a second-order FM transition, the scaling analysis of $-\Delta S_M$ can also be expressed as

$$-\Delta S_M \propto H^n g\left(\frac{\varepsilon}{H^{1/(\beta+\gamma)}}\right), \tag{18}$$

where n, β, and γ denote critical exponents and $g(x)$ is a scaling function [70]. With appropriately selected critical exponents, the plots of $\frac{-\Delta S_M(T)}{H^n}$ vs $\frac{\varepsilon}{H^{1/(\beta+\gamma)}}$ should collapse onto a single curve, which is indeed observed in the inset of Fig. 9(b). The well-scaled $-\Delta S_M(T, H)$ curves verify the reliability and validity of the acquired critical exponents.

To provide further insight into the important role of the anisotropy in $LaCrSb_3$, we calculated the magnetocrystalline anisotropy constant K_u, which is related to the saturation magnetization M_s and the saturation field H_s under the $H \| ab$ plane, i.e., $2K_u/M_s = \mu_0 H_s$, where μ_0 denotes the vacuum permeability [71]. As displayed in the left axis of Fig. 10, the derived K_u is found to be temperature dependent, gradually decreasing with an increasing temperature. This tendency could arise from local spin clusters fluctuating randomly around the macroscopic magnetization vector and activated by a nonzero thermal energy [72,73]. The magnitude of K_u in $LaCrSb_3$ is equal to 74.9 kJ/m^3 at $T = 67$ K, which is comparable with that of typical low dimensional ferromagnets $NdCrGe_3$ [68], VI_3 [61] and $CrGeTe_3$ [74]. According to a classical theory, $\langle K^n \rangle \propto M_s^{n(n+1)/2}$, where $\langle K^n \rangle$ denotes the anisotropy expectation value for the nth power angular function [72,73], in the case of an uniaxial anisotropy and

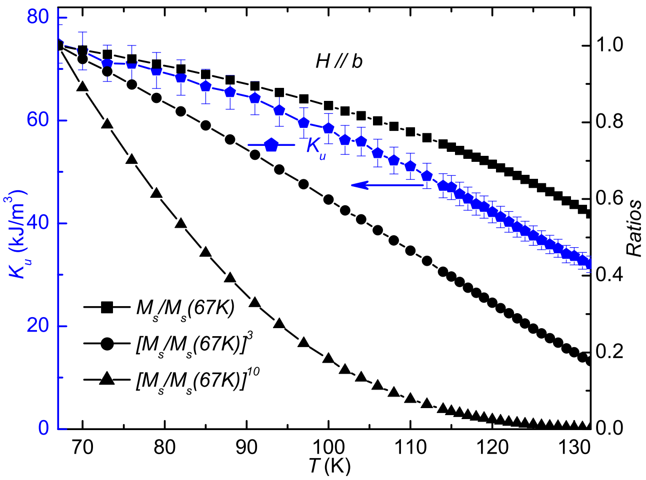

FIG. 10. (a) The temperature dependence of the anisotropy constant K_u (left axis) and the ratios of $[M_s/M_s(67K)]^{n(n+1)/2}$ with $n = 1$, 2, and 4 (right axis).

a cubic anisotropy $n = 2$ and 4, resulting in an exponent of 3 and 10, respectively. The temperature dependence of $[M_s/M_s(67K)]^{n(n+1)/2}$ with $n = 1, 2,$ and 4 are displayed in the right axis of Fig. 10. The comparison in Fig. 10 demonstrates the anisotropy in $LaCrSb_3$ is different from both an uniaxial anisotropy and a cubic anisotropy, which is consistent with the anisotropic magnetic entropy change and could be due to the complex magnetic structure in $LaCrSb_3$.

For the investigation and modulation of topological properties in $LaCrSb_3$, the clarification of the magnetic interactions and/or the magnetic structure is of great importance [75]. It is known that the spin-orbital coupling and magnetic interaction play essential roles in the formation and evolution of topological nontrivial states and in the process of anomalous Hall effect. In PrAlGe, the intrinsic FM ordering induces the split of bands, which makes the Weyl nodes in k space shift to break time-reversal symmetry, generating a large anomalous Hall effect [75,76]. In CeAlGe, it has been confirmed that many magnetic incommensurate phases exists, implying close relations between magnetism and topologically nontrivial states [77]. Furthermore, it is proposed that a Dirac semimetal state exists in the AFM ground state and a Weyl semimetal state appears in the FM state in rare-earth monopnictides NdSb [78,79]. Thus, the comprehensive investigation of the magnetism in $LaCrSb_3$ is significant for understanding the interplay between the magnetism and nontrivial band topology features and offering explanations to the AHC in $LaCrSb_3$.

IV. CONCLUSIONS

In summary, a systematic investigation on the critical behavior and magnetocaloric effect of $LaCrSb_3$ around its PM-FM phase transition are performed. Critical behavior analysis clarifies that the ferromagnetic transition is of second order. The critical exponents $\beta = 0.298(7)$, $\gamma = 1.277(9)$, and $\delta = 5.28(9)$ are generated with various methods, including the modified Arrott plot, the KF method, the Widom scaling law, and critical isotherm analysis. The self-consistency and reliability of obtained critical exponents are confirmed by the scaling analysis. A 3D critical behavior is verified. The spin interaction in $LaCrSb_3$ is of a long range and the exchange interaction decays with distance as $J(r) = r^{-4.9}$. Moreover, strong magnetocrystalline anisotropy is confirmed in magnetic entropy change. The $-\Delta S_M^{\max}(H)$ as well as the field-dependent RCP follow the power law behavior. The scaling analysis of magnetic entropy change $-\Delta S_M(T, H)$ demonstrates the accurate estimation of critical exponents. Considering the strong magnetocrystalline anisotropy, the long-range magnetic interaction, and the strong Berry coverture of $LaCrSb_3$, further theoretic calculation and experimental investigation are of great interest and urgently needed.

ACKNOWLEDGMENTS

This work was supported by the National Natural Science Foundation of China (Grant No. 11804141), the Natural Science Foundation of Henan Province (Grant No. 212300410375), the Key scientific research projects of Henan Province (Grant No. 21A140018), the Youth Backbone Teacher of Henan Province (Grant No. 2020GGJS197), and the college students innovations special project (Grants No. 202110482016, No. 202110482022, and No. 202110482028).

[1] M. K. Wu, J. R. Ashburn, C. J. Torng, P. H. Hor, R. L. Meng, L. Gao, Z. J. Huang, Y. Q. Wang, and C. W. Chu, Phys. Rev. Lett. **58**, 908 (1987).

[2] J. G. Bednorz and K. A. Muller, Z. Phys. B **64**, 189 (1986).

[3] Y. Kamihara, T. Watanabe, M. Hirano, and H. Hosono, J. Am. Chem. Soc. **130**, 3296 (2008).

[4] A. C. Masset, C. Michel, A. Maignan, M. Hervieu, O. Toulemonde, F. Studer, B. Raveau, and J. Hejtmanek, Phys. Rev. B **62**, 166 (2000).

[5] I. Terasaki, Y. Sasago, and K. Uchinokura, Phys. Rev. B **56**, R12685 (1997).

[6] R. M. Kusters, J. Singleton, D. A. Keen, R. McGreevy, and W. Hayes, Phys. B (Amsterdam, Neth.) **155**, 362 (1989).

[7] C. Gong, L. Li, Z. L. Li, H. W. Ji, A. Stern, Y. Xia, T. Cao, W. Bao, C. Z. Wang, Y. Wang, Z. Q. Qiu, R. J. Cava, S. G. Louie, J. Xia, and X. Zhang, Nature (London) **546**, 265 (2017).

[8] B. Huang, G. Clark, E. Navarro-Moratalla, D. R. Klein, R. Cheng, K. L. Seyler, D. Zhong, E. Schmidgall, M. A. McGuire, D. H. Cobden, W. Yao, D. Xiao, P. Jarillo-Herrero, and X. D. Xu, Nature (London) **546**, 270 (2017).

[9] M. Bonilla, S. Kolekar, Y. J. Ma, H. C. Diaz, V. Kalappattil, R. Das, T. Eggers, H. R. Gutierrez, M. H. Phan, and M. Batzill, Nat. Nanotechnol. **13**, 289 (2018).

[10] A. K. Geim and I. V. Grigorieva, Nature (London) **499**, 419 (2013).

[11] J. Lee, S. Lee, J. H. Ryoo, S. Kang, T. Y. Kim, P. Kim, C. Park, J. Park, and H. Cheong, Nano Lett. **16**, 7433 (2016).

[12] K. S. Novoselov, A. Mishchenko, A. Carvalho, and A. H. Castro Neto, Science **353**, aac9439 (2016).
[13] D. J. O'Hara, T. Zhu, A. H. Trout, A. S. Ahmed, Y. K. Luo, C. H. Lee, M. R. Brenner, S. Rajan, J. A. Gupta, D. W. McComb, and R. K. Kawakami, Nano Lett. **18**, 3125 (2018).
[14] Y. J. Deng, Y. J. Yu, Y. C. Song, J. Z. Zhang, N. Z. Wang, Z. Y. Sun, Y. F. Yi, Y. Z. Wu, S. W. Wu, J. Y. Zhu, J. Wang, X. H. Chen, and Y. B. Zhang, Nature (London) **563**, 94 (2018).
[15] N. D. Mermin and H. Wagner, Phys. Rev. Lett. **17**, 1133 (1966)
[16] D. D. Jackson, M. Torelli, and Z. Fisk, Phys. Rev. B **65**, 014421 (2001).
[17] M. Inamdar, A. Thamizhavel, and S. Ramakrishnan, J. Phys.: Condens. Matter **20**, 295226 (2008).
[18] S. J. Crerar, L. Deakin, and A. Mar, Chem. Mater. **17**, 2780 (2005).
[19] N. P. Raju, J. E. Greedan, M. J. Ferguson, and A. Mar, Chem. Mater. **10**, 3630 (1998).
[20] E. Granado, H. Martinho, M. S. Sercheli, P. G. Pagliuso, D. D. Jackson, M. Torelli, J. W. Lynn, C. Rettori, Z. Fisk, and S. B. Oseroff, Phys. Rev. Lett. **89**, 107204 (2002).
[21] N. Kumar, N. Lamba, J. Gayles, C. Le, P. Vir, S. N. Guin, Y. Sun, C. Felser, and C. Shekhar, Adv. Quantum Technol. **4**, 2100023 (2021).
[22] M. E. Fisher, Rev. Mod. Phys. **46**, 597 (1974).
[23] H. E. Stanley, Rev. Mod. Phys. **71**, S358 (1999).
[24] Y. Liu, Z. Hu, E. Stavitski, K. Attenkofer, and C. Petrovic, Phys. Rev. B **103**, 144432 (2021).
[25] Y. Liu, Z. Hu, E. Stavitski, K. Attenkofer, and C. Petrovic, Phys. Rev. Research **3**, 023181 (2021).
[26] E. P. Wohlfarth, J. Magn. Magn. Mater. **7**, 113 (1978).
[27] T. Moriya, J. Magn. Magn. Mater. **14**, 1 (1979).
[28] Z. E. Brubaker, J. S. Harvey, J. R. Badger, R. R. Ullah, D. J. Campbell, Y. Xiao, P. Chow, C. Kenney-Benson, J. S. Smith, C. Reynolds, J. Paglione, R. J. Zieve, J. R. Jeffries, and V. Taufour, Phys. Rev. B **101**, 214408 (2020).
[29] E. C. Stoner, Phil. Mag. **15**, 1018 (1933).
[30] M. Leonard, S. Saha, and N. Ali, J. Appl. Phys. **85**, 4759 (1999).
[31] A. Arrott, Phys. Rev. **108**, 1394 (1957).
[32] S. K. Banerjee, Phys. Lett. **12**, 16 (1964).
[33] H. E. Stanley, *Introduction to Phase Transitions and Critical Phenomena* (Oxford University Press, London, 1971).
[34] M. E. Fisher, Rep. Prog. Phys. **30**, 615 (1967).
[35] A. K. Pramanik and A. Banerjee, Phys. Rev. B **79**, 214426 (2009).
[36] X. Yang, J. Pan, S. Liu, M. Yang, L. Cao, D. Chu, and K. Sun, Phys. Rev. B **103**, 104405 (2021).
[37] X. Yang, J. Pan, K. Sun, Y. Shi, L. Cao, S. Liu, W. Gai, D. Chu, and M. Yang, J. Alloys Compd. **886**, 161118 (2021).
[38] J. S. Kouvel and M. E. Fisher, Phys. Rev. **136**, A1626 (1964).
[39] B. Widom, J. Chem. Phys. **43**, 3898 (1965).
[40] J. C. LeGuillou and J. Zinn-Justin, Phys. Rev. B **21**, 3976 (1980).
[41] A. Taroni, S. T. Bramwell, and P. C. Holdsworth, J. Phys.: Condens. Matter **20**, 275233 (2008).
[42] T. Kong, K. Stolze, D. Ni, S. K. Kushwaha, and R. J. Cava, Phys. Rev. Mater. **2**, 014410 (2018).
[43] S. Dash, A. V. Lukoyanov, Y. V. Knyazev, Y. I. Kuźmin, E. D. Baglasov, B. Weise, P. Kumar, M. Vasundhara, and A. K. Patra, Phys. Chem. Chem. Phys. **21**, 10823 (2019).
[44] N. T. M. Duc, C. M. Hung, N. T. Huong, and M. H. Phan, J. Electron. Mater. **49**, 2596 (2020).
[45] R. Caballero-Flores, N. S. Bingham, M. H. Phan, M. A. Torija, C. Leighton, V. Franco, A. Conde, T. L. Phan, S. C. Yu, and H. Srikanth, J. Phys.: Condens. Matter **26**, 286001 (2014).
[46] M. Haug, M. Fähnle, H. Kronmüller, and F. Haberey, J. Magn. Magn. Mater. **69**, 163 (1987).
[47] A. Tozri, E. Dhahri, E. K. Hlil, and M. A. Valente, Solid State Commun. **151**, 315 (2011).
[48] M. H. Phan, V. Franco, A. Chaturvedi, S. Stefanoski, G. S. Nolas, and H. Srikanth, Phys. Rev. B **84**, 054436 (2011).
[49] R. P. Madhogaria, R. Das, E. M. Clements, V. Kalapattil, M. H. Phan, H. Srikanth, N. T. Dang, D. P. Kozlenko, and N. S. Bingham, Phys. Rev. B **99**, 104436 (2019).
[50] P. Lampen, M. H. Phan, H. Srikanth, K. Kovnir, P. Chai, and M. Shatruk, Phys. Rev. B **90**, 174404 (2014).
[51] P. Zhang, P. Lampen, T. L. Phan, S. C. Yu, T. D. Thanh, N. H. Dan, V. D. Lam, H. Srikanth, and M. H. Phan, J. Magn. Magn. Mater. **348**, 146 (2013).
[52] S. F. Fischer, S. N. Kaul, and H. Kronmuller, Phys. Rev. B **65**, 064443 (2002).
[53] M. E. Fisher, S. Ma, and B. G. Nickel, Phys. Rev. Lett. **29**, 917 (1972).
[54] G. T. Lin, X. Luo, F. C. Chen, J. Yan, J. J. Gao, Y. Sun, W. Tong, P. Tong, W. J. Lu, Z. G. Sheng, W. H. Song, X. B. Zhu, and Y. P. Sun, Appl. Phys. Lett. **112**, 072405 (2018).
[55] B. Liu, Y. Zou, L. Zhang, S. Zhou, Z. Wang, W. Wang, Z. Qu, and Y. Zhang, Sci. Rep. **6**, 33873 (2016).
[56] G. T. Lin, H. L. Zhuang, X. Luo, B. J. Liu, F. C. Chen, J. Yan, Y. Sun, J. Zhou, W. J. Lu, P. Tong, Z. G. Sheng, Z. Qu, W. H. Song, X. B. Zhu, and Y. P. Sun, Phys. Rev. B **95**, 245212 (2017).
[57] E. M. Clements, R. Das, L. Li, P. J. Lampen-Kelley, M. H. Phan, V. Keppens, D. Mandrus, and H. Srikanth, Sci. Rep. **7**, 6545 (2017).
[58] Y. Liu, R. J. Koch, Z. Hu, N. Aryal, E. Stavitski, X. Tong, K. Attenkofer, E. S. Bozin, W. Yin, and C. Petrovic, Phys. Rev. B **102**, 085158 (2020).
[59] V. Franco, A. Conde, M. D. Kuzmin, and J. M. Romero-Enrique, J. Appl. Phys. **105**, 07A917 (2009).
[60] Z. Z. Jiang, X. Luo, J. Yan, J. J. Gao, W. Wang, G. C. Zhao, Y. Sun, J. G. Si, W. J. Lu, P. Tong, X. B. Zhu, W. H. Song, and Y. P. Sun, Phys. Rev. B **102**, 144433 (2020).
[61] J. Yan, X. Luo, F. C. Chen, J. J. Gao, Z. Z. Jiang, G. C. Zhao, Y. Sun, H. Y. Lv, S. J. Tian, Q. W. Yin, H. C. Lei, W. J. Lu, P. Tong, W. H. Song, X. B. Zhu, and Y. P. Sun, Phys. Rev. B **100**, 094402 (2019).
[62] Y. Sun, Z. Song, Q. Tang, and X. Luo, J. Phys. Chem. C **124**, 11110 (2020).
[63] K. A. Gschneidner Jr., V. K. Pecharsky, A. O. Pecharsky, and C. B. Zimm, Mater. Sci. Forum **315**, 69 (1999).
[64] H. Oesterreicher and F. T. Parker, J. Appl. Phys. **55**, 4334 (1984).
[65] V. Franco, J. S. Blazquez, and A. Conde, Appl. Phys. Lett. **89**, 222512 (1984).
[66] V. Franco, R. Caballero-Flores, A. Conde, Q. Y. Dong, and H. W. Zhang, J. Magn. Magn. Mater. **321**, 1115 (2009).
[67] W. Liu, Y. Wang, J. Fan, L. Pi, M. Ge, L. Zhang, and Y. Zhang, Phys. Rev. B **100**, 104403 (2019).

[68] X. Yang, J. Pan, Y. Shi, K. Sun, L. Cao, and W. Sun, J. Phys. Chem. C **125**, 23370 (2021).

[69] V. Franco and A. Conde, Int. J. Refrig. **33**, 465 (2010).

[70] Y. Su, Y. Sui, J. G. Cheng, J. S. Zhou, X. Wang, Y. Wang, and J. B. Goodenough, Phys. Rev. B **87**, 195102 (2013).

[71] B. D. Cullity and C. D. Graham, *Introduction to Magnetic Materials* (Wiley, Hoboken, NJ, 2009).

[72] C. Zener, Phys. Rev. **96**, 1335 (1954).

[73] W. J. Carr, J. Appl. Phys. **29**, 436 (1958).

[74] Y. Liu and C. Petrovic, Phys. Rev. Mater. **3**, 014001 (2019).

[75] W. Liu, J. Zhao, F. Meng, A. Rahman, Y. Qin, J. Fan, L. Pi, Z. Tian, H. Du, L. Zhang, and Y. Zhang, Phys. Rev. B **103**, 214401 (2021).

[76] G. Chang, B. Singh, S.-Y. Xu, G. Bian, S.-M. Huang, C.-H. Hsu, I. Belopolski, N. Alidoust, D. S. Sanchez, H. Zheng, H. Lu, X. Zhang, Y. Bian, T.-R. Chang, H.-T. Jeng, A. Bansil, H. Hsu, S. Jia, T. Neupert, H. Lin *et al.*, Phys. Rev. B **97**, 041104(R) (2018).

[77] P. Puphal, V. Pomjakushin, N. Kanazawa, V. Ukleev, D. J. Gawryluk, J. Ma, M. Naamneh, N. C. Plumb, L. Keller, R. Cubitt, E. Pomjakushina, and J. S. White, Phys. Rev. Lett. **124**, 017202 (2020).

[78] M. Neupane, M. M. Hosen, I. Belopolski, N. Wakeham, K. Dimitri, N. Dhakal, J.-X. Zhu, M. Z. Hasan, E. D. Bauer, and F. Ronning, J. Phys.: Condens. Matter **28**, 23LT02 (2016).

[79] Y. Wang, J. H. Yu, Y. Q. Wang, C. Y. Xi, L. S. Ling, S. L. Zhang, J. R. Wang, Y. M. Xiong, T. Han, H. Han, J. Yang, J. Gong, L. Luo, W. Tong, L. Zhang, Z. Qu, Y. Y. Han, W. K. Zhu, L. Pi, X. G. Wan *et al.* Phys. Rev. B **97**, 115133 (2018).